PID Flight Control of a Paraglider toward Spacecraft Retrieval

Yoshimasa Ochi
National Defense Academy, Japan

Abstract: A paraglider with a guidance and control capability can be used for retrieval of a spacecraft. Design of a guidance and control system for a paraglider requires its dynamic model and an appropriate control design scheme. This paper presents nonlinear and linear models developed by the author and design of a PID flight control system also based on the method proposed by the author. The model-based design approach easily provides a controller with good control performance and adequate stability margin, which can be traded off with each other through design parameters. A design example and numerical simulation results for a manned paraglider are shown.

宇宙機回収のためのパラグライダーの PID 飛行制御

越智　徳昌
防衛大学校

摘要：誘導制御機能をもったパラグライダーは宇宙機の回収に利用できる．パラグライダーのための誘導制御システムの設計にはその運動モデルと適当な制御系設計手法が必要である．本稿では，著者によって開発された非線形及び線形モデルと PID 飛行制御系の設計について述べる．このモデルは内力を解析的に消去した状態方程式で与えられ，このモデルと積分型最適サーボに基づく PID 制御系の設計法を用いて，飛行制御系を設計する．この設計法の特徴は望ましい制御性能と十分な安定余裕をもつ PID ゲインが容易に得られることであり，さらに設計パラメータを用いて制御性能と安定余裕のトレードオフを行うことが可能である．有人用パラグライダーに対する設計例と数値シミュレーション結果によりその有効性を示す.

1. Introduction

A paraglider is a kind of parachute, which is basically used for deceleration. Unlike a conventional round-type parachute, a square-type parafoil, which is often used for sky diving, has a good controllability. Particularly, a paraglider with a larger aspect ratio has an excellent gliding performance and maneuver-ability like a glider in addition to the controllability. Thus, paragliding has become a popular sport in the sky and a manned-powered paraglider is used for aerial photographing as well as hobby. Providing a paraglider with a guidance and control capability makes it an unmanned aerial vehicle (UAV), which can also be used for airdrop and hence for spacecraft retrieval. Actually, the X-38 was equipped with a paraglider having a 700m^2-canopy, which carried the 9-ton vehicle to the landing area and made a safe landing[1)]. Such a UAV inevitably requires a guidance and control system. Although the author has no detailed information on how the guidance and control system for the X-38 retrieval was designed, usually a reliable dynamic model and an appropriate control design method are required for model-based control design. Of course, there are model-free design methods, such as fuzzy control, artificial neural network control, or PID control with trial-and-error gain selection. The model-free approach is effective and necessary for a plant whose dynamics is completely unknown or difficult to be modeled. However, if not so, the model-based approach should be taken, because it not only reasonably provides a controller satisfying specified properties but also tells the designer why the required control performance is achieved and how to modify the controller if not achieved.

This paper presents a dynamic model of a paraglider[2)] and PID controller design[3)] based on the model. Both of the mathematical model and controller design method are developed by the author. This paper is organized as follows. In Section 2, an outline of modeling of the parafoil dynamics is given. In Section 3, the PID controller design method is

described, and Section 4 shows a design example and nonlinear simulation results. Finally, Section 5 gives summary and conclusions.

2. Modeling of Paraglider Dynamics

2.1 Nonlinear state equation

There are many researches on modeling of parafoil dynamics. A typical configuration of a parafoil is the one composed of a canopy and a payload, where the suspension lines and the payload are connected at two joints. This configuration allows the paraglider to be modeled to have eight degrees of freedom (8-DOF) of motion, and also formulate the modeling as a two-body problem, where it is difficult how to deal with the internal force or tension in the suspension lines. The internal forces should be eliminated to obtain a complete dynamic model. However, to the best of the author's knowledge, no report has been published in which exact elimination of the internal forces is mentioned, and even when mentioned, the forces are approximately eliminated in numerical simulation. By contrast, the dynamics model developed by the present author does not include the tension, which is analytically eliminated from the equations of motion. Hence, the model is described as a state equation. To derive the state equation, consider the following three sets of state equations regarding linear motion, angular motion, and the kinematic relations between the angular velocities and Euler angles, respectively:

$$\boldsymbol{E}_F \dot{\boldsymbol{x}}_c = \boldsymbol{F}_F , \tag{1}$$

$$\boldsymbol{E}_M \dot{\boldsymbol{x}}_c = \boldsymbol{F}_M , \tag{2}$$

$$\boldsymbol{E}_K \dot{\boldsymbol{x}}_c = \boldsymbol{F}_K , \tag{3}$$

where $\boldsymbol{x}_c = [u_c\ v_c\ w_c\ p_c\ q_c\ r_c\ q_{pc}\ r_{pc}\ \theta_{pc}\ \psi_{pc}\ \phi_c\ \theta_c]^T$ is a state vector, and the state variables, u_c, v_c, and w_c, are forward, sideward, and downward speed (m/s), respectively, in the canopy body-axis coordinate system; p_c, q_c, and r_c are roll, pitch, and yaw rates (rad/s), respectively; q_{pc} and r_{pc} are pitch and yaw rates (rad/s) of the canopy relative to the payload; θ_{pc} and ψ_{pc} are pitch and yaw angles of the canopy relative to the payload; ϕ_c and θ_c are roll and pitch angles of the canopy, and the matrices, $\boldsymbol{E}_F$ and $\boldsymbol{E}_M$, and the vectors, $\boldsymbol{F}_F$, $\boldsymbol{F}_M$, and $\boldsymbol{F}_K$, are nonlinear functions of the state and input variables. The inputs are the right and left canopy deflection (called brake) angles (rad), δ_R and δ_L, and thrust (N), δ_{th}, generated at the payload with a power unit and a propeller. The trailing edge of the canopy on the right and left sides can be deflected by pulling the control lines. $\boldsymbol{E}_K$ is a constant matrix. All the variables are defined in the body-axis coordinate system of the canopy.

The right-hand sides of Eqs. (1) and (2) include the internal forces acting at the joints between the canopy and the payload. It was found that multiplying the combined eqtuation of Eqs. (1) and (2) from the left with the matrix:

$$\boldsymbol{C}_M = \begin{bmatrix} \cos\theta_{pc}\cos\psi_{pc} & 0 & \sin\theta_{pc}\cos\psi_{pc} & 1 & 0 & 0 \\ \cos\theta_{pc}\sin\psi_{pc} & 0 & \sin\theta_{pc}\sin\psi_{pc} & 0 & 1 & 0 \\ 0 & 1 & 0 & 0 & 0 & 0 \\ -\sin\theta_{pc} & 0 & \cos\theta_{pc} & 0 & 0 & 1 \\ 0 & 0 & 0 & 0 & 0 & 1 \end{bmatrix}$$

eliminates the internal forces. This manipulation and adding Eq. (3) yields the state equation of motion:

$$\dot{\boldsymbol{x}}_c = \boldsymbol{E}^{-1}\boldsymbol{F} . \tag{4}$$

If the right-hand side of Eq. (1) is affine with respect to the control inputs, then the state equation can be rewritten as

$$\dot{\boldsymbol{x}}_c = \boldsymbol{f}(\boldsymbol{x}_c) + \boldsymbol{g}(\boldsymbol{x}_c)\boldsymbol{u} , \tag{5}$$

where $\boldsymbol{u} = [\delta_e\ \delta_r\ \delta_{th}]^T$. The collective and differential deflection angles, δ_e and δ_r, are defined as $\delta_e = \delta_R + \delta_L$ and $\delta_e = \delta_R - \delta_L$, respectively.

2.2 Linear state equation

Either analytically or numerically applying the first-order approximation of Taylor series expansion to the nonlinear state equation yields the linear state equation:

$$\Delta\dot{\boldsymbol{x}}_c = \boldsymbol{A}_c\Delta\boldsymbol{x}_c + \boldsymbol{B}_c\Delta\boldsymbol{u} , \tag{6}$$

where the small perturbation of the variables from the equilibrium ones, $\boldsymbol{x}_c^*$ and $\boldsymbol{u}^*$, are defined as $\Delta\boldsymbol{x}_c = \boldsymbol{x}_c - \boldsymbol{x}_c^*$ and $\Delta\boldsymbol{u} = \boldsymbol{u} - \boldsymbol{u}^*$, and $\boldsymbol{A}_c$ and $\boldsymbol{B}_c$ are constant derivative matrices. The linear system described by Eq. (6) can be separated into two decoupled systems, i.e., the longitudinal motion and the lateral-directional motion, respectively, as

$$\Delta\dot{\boldsymbol{x}}_{clong} = \boldsymbol{A}_{clong}\Delta\boldsymbol{x}_{clong} + \boldsymbol{B}_{clong}\Delta\boldsymbol{u}_{long} , \tag{7}$$

$$\Delta\dot{\boldsymbol{x}}_{clat} = \boldsymbol{A}_{clat}\Delta\boldsymbol{x}_{clat} + \boldsymbol{B}_{clat}\Delta u_{lat} , \tag{8}$$

where $\Delta\boldsymbol{x}_{clong} = [\Delta u_c\ \Delta w_c\ \Delta q_c\ \Delta q_{pc}\ \Delta\theta_{pc}\ \Delta\theta_c]^T$, $\Delta\boldsymbol{u}_{long} = [\Delta\delta_e\ \Delta\delta_{th}]^T$, $\Delta\boldsymbol{x}_{clat} = [\Delta v_c\ \Delta p_c\ \Delta r_c\ \Delta r_{pc}\ \Delta\psi_{pc}\ \Delta\phi_c]^T$, and $\Delta u_{lat} = \Delta\delta_r$.

2.3 State transformation

The above nonlinear and linear state equations are described with the state variables of the canopy. However, the state equations expressed with the state variables of the payload is desired as a dynamic model for control system design, since sensors and the propelling unit are mounted on the payload. Meanwhile, the geometric constraint of the 8-DOF two-body system allows the motion of the payload to be uniquely determined from the motion of the canopy and the motion of the payload relative to the canopy, and vice versa. This means that the dynamics of the paraglider can be represented with the state variables of the payload motion and the relative motion. Actually this is possible in the case of linearized system. The linear relation between the canopy states and the payload states can be derived by linearization of nonlinear relations between the canopy and payload states. Thus, the state transformation matrix, $\boldsymbol{T}$, is obtained for the linear state variables, i.e.,

$$\Delta \boldsymbol{x}_p = \boldsymbol{T}\Delta \boldsymbol{x}_c, \tag{9}$$

where $\Delta \boldsymbol{x}_p$ is a small perturbation of $\boldsymbol{x}_p = [u_p\ v_p\ w_p\ p_p\ q_p\ r_p\ q_{pc}\ r_{pc}\ \theta_{pc}\ \psi_{pc}\ \phi_p\ \theta_p]^T$, and the subscript, '$p$', denotes the payload states.

3. Controller Design

3.1 Plant model reduction

Consider a linear time-invariant system given by

$$\dot{\boldsymbol{x}} = \boldsymbol{A}\boldsymbol{x} + \boldsymbol{B}\boldsymbol{u}\,, \tag{10}$$

$$\boldsymbol{y} = \boldsymbol{C}\boldsymbol{x}, \tag{11}$$

where $\boldsymbol{x} \in \Re^n$ is a state vector, $\boldsymbol{u} \in \Re^p$ is an input vector, and $\boldsymbol{y} \in \Re^p$ is an output vector. This system is assumed to be stabilizable and detectable, and $\boldsymbol{C}$ is assumed to be of row full rank.

Express the system in the form of normalized right coprime factorization (NRCF), [4] i.e.,

$$\boldsymbol{P}(s) = \boldsymbol{N}(s)\boldsymbol{M}(s)^{-1} = \boldsymbol{C}(s\boldsymbol{I} - \boldsymbol{A})^{-1}\boldsymbol{B} =: \left[\begin{array}{c|c} \boldsymbol{A} & \boldsymbol{B} \\ \hline \boldsymbol{C} & 0 \end{array}\right], \tag{12}$$

where $\boldsymbol{N}(s)$ and $\boldsymbol{M}(s)$ are given by

$$\begin{bmatrix} \boldsymbol{M}(s) \\ \boldsymbol{N}(s) \end{bmatrix} = \left[\begin{array}{c|c} \boldsymbol{A}+\boldsymbol{B}\boldsymbol{F} & \boldsymbol{B} \\ \hline \boldsymbol{F} & \boldsymbol{I} \\ \boldsymbol{C} & 0 \end{array}\right]. \tag{13}$$

In Eq. (13), $\boldsymbol{F} = -\boldsymbol{B}^T\boldsymbol{X}$ and $\boldsymbol{X}$ is the positive definite solution of the algebraic Riccati equation:

$$\boldsymbol{X}\boldsymbol{A} + \boldsymbol{A}^T\boldsymbol{X} - \boldsymbol{X}\boldsymbol{B}\boldsymbol{B}^T\boldsymbol{X} + \boldsymbol{C}^T\boldsymbol{C} = 0. \tag{14}$$

Applying balanced truncation[5] to the system of Eq. (13) yields the reduced order system:

$$\begin{bmatrix} \boldsymbol{M}_r(s) \\ \boldsymbol{N}_r(s) \end{bmatrix} = \left[\begin{array}{c|c} \boldsymbol{A}_{Fr} & \boldsymbol{B}_r \\ \hline \boldsymbol{F}_r & \boldsymbol{I} \\ \boldsymbol{C}_r & 0 \end{array}\right]. \tag{15}$$

From the truncated system, the following reduced order plant model is obtained:

$$\dot{\boldsymbol{x}}_r = \boldsymbol{A}_r\boldsymbol{x}_r + \boldsymbol{B}_r\boldsymbol{u}\,, \tag{16}$$

$$\boldsymbol{y} = \boldsymbol{C}_r\boldsymbol{x}_r, \tag{17}$$

where $\boldsymbol{A}_r = \boldsymbol{A}_{Fr} - \boldsymbol{B}_r\boldsymbol{F}_r$. This model reduction method is called fractional balanced reduction (FBR).[6]

3.2 State transformation

Define a new state vector as

$$\boldsymbol{z} = \begin{bmatrix} \boldsymbol{y}^T & \dot{\boldsymbol{y}}^T \end{bmatrix}^T. \tag{18}$$

The state vector can be written as

$$\boldsymbol{z} = \boldsymbol{M}_s\boldsymbol{x}_r + \boldsymbol{N}_s\boldsymbol{u}, \tag{19}$$

where

$$\boldsymbol{M}_s = \begin{bmatrix} \boldsymbol{C}_r^T & (\boldsymbol{C}_r\boldsymbol{A}_r)^T \end{bmatrix}^T, \tag{20}$$

$$\boldsymbol{N}_s = \begin{bmatrix} 0^T & (\boldsymbol{C}_r\boldsymbol{B}_r)^T \end{bmatrix}^T. \tag{21}$$

$\boldsymbol{M}_s$ is assumed to be nonsingular. Then, Eq. (19) can further be rewritten as

$$\boldsymbol{x}_r = \boldsymbol{M}_s^{-1}(\boldsymbol{z} - \boldsymbol{N}_s\boldsymbol{u}). \tag{22}$$

Substituting Eq. (22) into Eq. (16) yields

$$\dot{\boldsymbol{z}} = \boldsymbol{A}_s\boldsymbol{z}_s + \boldsymbol{B}_s\boldsymbol{u} + \boldsymbol{N}_s\dot{\boldsymbol{u}}\,, \tag{23}$$

where

$$\boldsymbol{A}_S = \boldsymbol{M}_S\boldsymbol{A}_r\boldsymbol{M}_S^{-1} \tag{24}$$

$$\boldsymbol{B}_S = -\boldsymbol{A}_S\boldsymbol{N}_S + \boldsymbol{M}_S\boldsymbol{B} \tag{25}$$

Consequently, the reduced plant model can be expressed with the state vector, $\boldsymbol{z}$, in the augmented state-space form as

$$\begin{bmatrix} \dot{\boldsymbol{z}} \\ \dot{\boldsymbol{u}} \end{bmatrix} = \begin{bmatrix} \boldsymbol{A}_s & \boldsymbol{B}_s \\ 0 & 0 \end{bmatrix}\begin{bmatrix} \boldsymbol{z} \\ \boldsymbol{u} \end{bmatrix} + \begin{bmatrix} \boldsymbol{N}_s \\ \boldsymbol{I} \end{bmatrix}\dot{\boldsymbol{u}}\,, \tag{26}$$

$$\boldsymbol{y} = \boldsymbol{C}_S[\boldsymbol{I}_n\ -\boldsymbol{N}_S][\boldsymbol{z}^T\ \boldsymbol{u}^T]^T, \tag{27}$$

where $\boldsymbol{C}_S = \boldsymbol{C}_r\boldsymbol{M}_S^{-1}$.

3.3 PID control law via integral-type optimal servo

Design an integral-type optimal servo[7] for the system given by Eqs. (26) and (27) as follows. First, define the further augmented system:

$$\frac{d}{dt}\begin{bmatrix}\dot{\boldsymbol{z}}\\ \dot{\boldsymbol{u}}\\ \boldsymbol{e}\end{bmatrix}=\begin{bmatrix}\boldsymbol{A}_s & \boldsymbol{B}_s & 0\\ 0 & 0 & 0\\ -\boldsymbol{C}_s & \boldsymbol{C}_s\boldsymbol{N}_s & 0\end{bmatrix}\begin{bmatrix}\dot{\boldsymbol{z}}\\ \dot{\boldsymbol{u}}\\ \boldsymbol{e}\end{bmatrix}+\begin{bmatrix}\boldsymbol{N}_s\\ \boldsymbol{I}\\ 0\end{bmatrix}\ddot{\boldsymbol{u}}, \tag{28}$$

where $\boldsymbol{e}$ (=$\boldsymbol{r}$–$\boldsymbol{y}$) is a control error vector and $\boldsymbol{r}$ is a constant reference output vector.

For the augmented system, the linear quadratic regulator (LQR) theory gives an optimal control law:

$$\dot{\boldsymbol{u}}=\boldsymbol{K}_z\boldsymbol{z}+\boldsymbol{K}_u\boldsymbol{u}+\boldsymbol{K}_e\int\boldsymbol{e}d\tau\,, \tag{29}$$

which minimizes the quadratic cost function:

$$J=\int_0^\infty\left(\dot{\boldsymbol{z}}^T\boldsymbol{Q}_z\dot{\boldsymbol{z}}+\dot{\boldsymbol{u}}^T\boldsymbol{Q}_u\dot{\boldsymbol{u}}+\boldsymbol{e}^T\boldsymbol{Q}\boldsymbol{e}+\ddot{\boldsymbol{u}}^T\boldsymbol{R}\ddot{\boldsymbol{u}}\right)dt\,, \tag{30}$$

where $\boldsymbol{Q}_z$ and $\boldsymbol{Q}_u$ are positive-semi-definite matrices, and $\boldsymbol{Q}$ and $\boldsymbol{R}$ are positive-definite matrices. With Laplace transform, the control law is rewritten as

$$\boldsymbol{u}=(s\boldsymbol{I}-\boldsymbol{K}_u)^{-1}\left(\boldsymbol{K}_{z0}\boldsymbol{y}+\boldsymbol{K}_{z1}s\boldsymbol{y}+\frac{\boldsymbol{K}_e}{s}\boldsymbol{e}\right)\cdot \tag{31}$$

Equation (31) can further be rewritten as

$$\boldsymbol{u}=\boldsymbol{K}_P\boldsymbol{y}+s(\boldsymbol{T}_ds+\boldsymbol{I})^{-1}\boldsymbol{K}_D\boldsymbol{y}+\frac{\boldsymbol{K}_I}{s}\boldsymbol{e}\,,\quad -\frac{1}{s}(\boldsymbol{T}_ds+\boldsymbol{I})^{-1}\boldsymbol{T}_d\boldsymbol{K}_I\boldsymbol{r} \tag{32}$$

where $\boldsymbol{T}_d=-\boldsymbol{K}_u^{-1}$, $\boldsymbol{K}_I=\boldsymbol{T}_d\boldsymbol{K}_e$, $\boldsymbol{K}_P=\boldsymbol{T}_d(\boldsymbol{K}_{z0}+\boldsymbol{K}_I)$, $\boldsymbol{K}_D=\boldsymbol{T}_d(\boldsymbol{K}_{z1}-\boldsymbol{K}_P)$. Removing the last term in Eq. (32) yields the I-PD control law:

$$\boldsymbol{u}=\boldsymbol{K}_P\boldsymbol{y}+s(\boldsymbol{T}_ds+\boldsymbol{I})^{-1}\boldsymbol{K}_D\boldsymbol{y}+\frac{\boldsymbol{K}_I}{s}\boldsymbol{e}\,\cdot \tag{33}$$

Note that removing the last term does not affect the closed-loop internal stability, since the term is given by the external input, $\boldsymbol{r}$.

The controller design procedure is summarized as follows.

1) Reduce the order of the plant to the 2p-th order with the FBR method, if n>2p.
2) Transform the state variables to obtain the augmented system expressed by Eqs. (26) and (27).
3) Design an IOS given by Eq. (32).
4) Convert the control law into the I-PD control law of Eq. (33).

The I-PD control law can be rewritten into the form of the PI-D or PID control law, respectively, as

$$\boldsymbol{u}=\left(-\boldsymbol{K}_P+\frac{\boldsymbol{K}_I}{s}\right)\boldsymbol{e}+s(\boldsymbol{T}_ds+\boldsymbol{I})^{-1}\boldsymbol{K}_D\boldsymbol{y} \tag{34}$$

$$\boldsymbol{u}=\left(-\boldsymbol{K}_P-s(\boldsymbol{T}_ds+\boldsymbol{I})^{-1}\boldsymbol{K}_D+\frac{\boldsymbol{K}_I}{s}\right)\boldsymbol{e} \tag{35}$$

by appropriately adding terms due the external input, $\boldsymbol{r}$, to the I-PD control law.

With numerical analysis software, MATLAB®, the first step of the design procedure can be carried out with the single function, 'ncfmr,' and an IOS can easily be designed by using the function, 'lqr'.

4. Design Example and Simulation

Consider a manned paraglider used for flight experiment[8], since the author does not have aerodynamic data of a parafoil for spacecraft retrieval. The canopy of the paraglider has the span of 9.95m and the chord length of 3.05m. The mass of the canopy is 6.4kg and the mass of the payload (the pilot and measurement unit) is 93.0kg. The trim airspeed is 9.54m/s, the trim angle of attack is 15.1deg, and the trim flight path angle is −11.4deg. The lift-to-drag ratio is 4.87.

The linear model expressed in the payload coordinate system is used for controller design. The outputs to be controlled are chosen to be the descent rate and the heading angle, which are controlled by the collective and differential brake angles, respectively.

The transfer function from the collective brake angle, δ_e, to the descent rate, $U_0\gamma$, where U_0 is a trim forward speed and γ is the flight path angle (positive for ascent), is given by

$$P_{P1}(s)=N_{P1}(s)/M_{P1}(s), \tag{36}$$

where

$$N_{P1}(s)=18.69(s+0.1672)(s^2+6.510s+12.36)\times(s^2+3.305s+4.999)$$

$$M_{P1}(s)=(s+0.5567)(s+1.958)(s^2+6.721s+15.17)\times(s^2+0.5698s+0.9665)$$

The reduced plant model obtained with FBR is

$$P_{C1}(s)=\frac{18.67s+6.763}{s^2+0.1603s+0.5320} \tag{37}$$

For the weighting matrices, Q_z =diag(10, 0), Q_u = 0, Q =1000, and R =1, the obtained PID gains are K_P = – 218.2, K_D = – 60.50, K_I = 87.32, and the time constant is T_d = 2.761.

The transfer function from the differential brake angle, δ_r, to the heading angle, $\beta_p + \psi_p$, where β_p and ψ_p is the sideslip and heading angles of the payload, respectively, is given by

$$P_{P2}(s) = N_{P2}(s)/M_{P2}(s), \tag{38}$$

where

$$N_{P2}(s) = 6.844\times10^{-3}(s+525.7)(s+0.3033) \times(s^2+1.325s+30.68)(s^2+2.489s+10.24)$$

$$M_{P2}(s) = s(s+1.347)(s+121.0)(s^2+0.2990s+25.35) \times(s^2+0.4488s+0.5698)$$

The reduced plant model obtained with FBR is

$$P_{C2}(s) = \frac{1.480}{s^2-0.1159s+0.3516}. \tag{39}$$

For the weighting matrices, Q_z =diag(0.1, 0.1), Q_u = 0, Q =0.1, and R =1, the obtained PID gains are K_P = –0.6472, K_D =–1.069, K_I =0.3162, and the time constant is T_d = 0.1000.

Thus, the two single-input single-output (SISO) PID controllers have been designed. Table 1 shows stability margins for the controllers along with the gain crossover frequency, ω_c. The results indicate that the controllers have adequate stability margins.

Table 1 Stability Margins

Breaking the loop at	Gain Margin	Phase Margin	ω_c (rad/s)
δ_e ($U_0\gamma$)	∞ (–13.68 dB)	61.60 deg	17.91
δ_r ($\beta_p+\psi_p$)	∞	48.94 deg	1.777

Numerical simulation has been conducted by applying the controllers to the nonlinear model given by Eq. (5). The controllers used here are in the form of the PID controller, i.e., Eq. (35). In order to avoid rapid change of the reference output, which causes large control input as well as unfavorable transient response, the reference output is filtered through a second-order-lag system before entering the closed loop. The second-order systems are $4/(s^2+4s+4)$ for the descent rate and $1/(s^2+2s+1)$ for the heading angle. It should be noted that the control lines can be pulled but cannot be pushed. This means that the negative control inputs cannot be applied, since the control inputs are zero at the trim flight condition. Therefore, the control inputs can frequently be saturated during flight control. The input saturation causes integral windup, resulting in a significant degradation of control performance. To prevent the integral windup, the anti-reset-wind-up compensation[9] is incorporated into the control system, i.e., the control law for the integral action is modified as

$$u_I(s) = \frac{1}{s}\{K_I e(s) + k(\tilde{u}-u(s))\}, \tag{40}$$

where k is an appropriate positive constant and $\tilde{u}$ is the output of the limiter. In this simulation, k is set to 10.

Figures 1 through 6 show time histories of the outputs, some of the state variables, and control inputs. The commanded maneuver is to turn to the right by 90deg and decrease the descent rate as small as possible. In order avoid input saturation, decrease of the descent rate by 0.3m/s is commanded during the right turn. When the right turn completes, the nominal trim flight is recovered in 10s, and then the descent rate is decreased to –1.15m/s for landing. The usable brake angle is less 0.3rad (17.19deg). Almost the maximum control inputs are applied to decrease the descent rate. Thanks to the appropriate reference outputs and the anti-reset-windup compensation, significant performance degradation due to input saturation does not occur. The time responses of the attitudes and the relative attitudes of the payload also indicate that the stable flight is achieved.

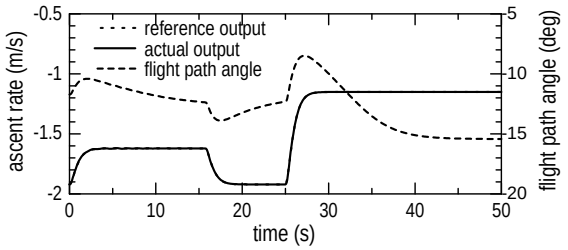

Fig. 1 Time histories of the ascent rate and flight path angle

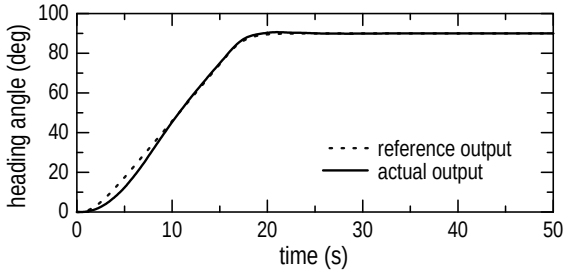

Fig. 2 Time history of the heading angle

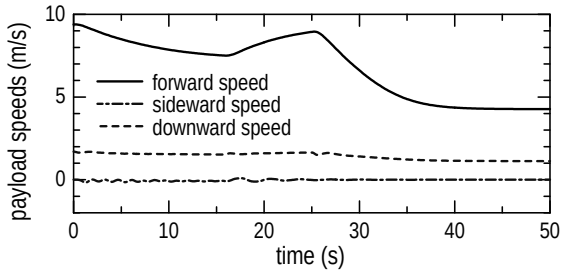

Fig. 3 Time histories of the speeds

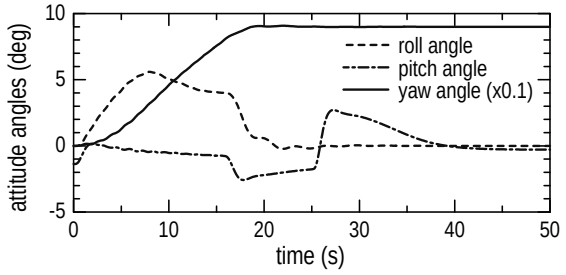

Fig. 4 Time histories of the Euler angles

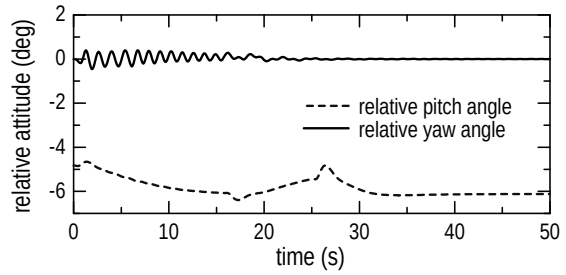

Fig. 5 Time histories of the relative attitudes

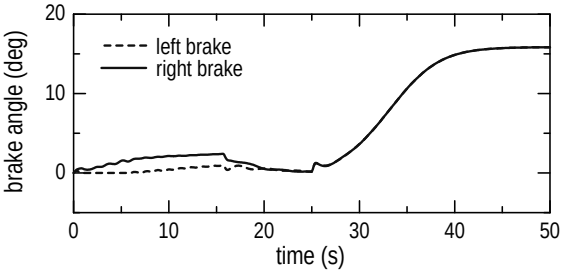

Fig. 6 Time histories of the brake angles

5. Conclusions

The model-based PID controller design has successfully provided a flight control system for the paraglider. Although the plant in the design example is a manned paraglider, the design method will probably be effective also for a paraglider-based retrieval system of a spacecraft.

References

1. J. Smith, T. Bennet, and R. Fox, “Development of the NASA X-38 parafoil landing system,” AIAA-99- 1730, pp. 205-217, 1999.
2. Y. Ochi and M. Watanabe, “Modelling and simulation of the dynamics of a powered paraglider,” Proceedings of Institution of Mechanical Engineering, Part G: Journal of Aerospace Engineering, Vol. 225, Issue 4, pp. 373-386, 2011.
3. H. Kondo, Y. Ochi, S. Sasano, “PID controller design using fractional balanced reduction,” Proceedings of SICE Annual Conference 2011, Tokyo, pp. 1791-1796, 2011
4. D. Meyer and G. Franklin, “A connection between coprime factorization and linear quadratic regulator theory,” *IEEE Trans. Automatic Control*, Vol. 32, pp. 227-228, 1987.
5. B. Moore, “Principal component analysis in linear systems: controllability, observability, and model reduction,” *IEEE Trans. Automatic Control*, Vol. 26, pp. 17-32, 1981.
6. D. Meyer, “Fractional balanced reduction: model reduction via fractional representation,” *IEEE Trans. Automatic Control*, Vol. 35, pp. 1341-1345, 1990.
7. H. Smith and E. Davison, “Design of industrial regulators,” *Proceedings IEE*, Vol. 119, pp. 1210- 1216, 1972.
8. A. Azuma, “Characteristics of paraglider,” JASPA, Tokyo, 1996. (in Japanese)
9. M. Kothare, P. Campo, M. Morari, and C. Nett, “A unified framework for the study of anti-windup design,” *Automatica*, Vol. 30, No. 12, pp. 1869-1883, 1994.